Applied Catalysis B: Environmental 308 (2022) 121215

Contents lists available at ScienceDirect

Applied Catalysis B: Environmental

journal homepage: www.elsevier.com/locate/apcatb

A visible-light-driven photocatalytic fuel cell/peroxymonosulfate (PFC/PMS) system using blue TiO_2 nanotube arrays (TNA) anode and Cu-Co-WO_3 cathode for enhanced oxidation of organic pollutant and ammonium nitrogen in real seawater

Jiaqi Sun [b], Lifen Liu [a,b,*], Fenglin Yang [b]

[a] Key Laboratory of Industrial Ecology and Environmental Engineering (MOE), School of Ocean Science and Technology, Dalian University of Technology, 124221 Dalian, Liaoning, China
[b] Key Laboratory of Industrial Ecology and Environmental Engineering (MOE), School of Environmental Science & Technology, Dalian University of Technology, 116024 Dalian, Liaoning, China

ARTICLE INFO

Keywords:
Catalytic electrodes
Photocatalytic fuel cell
PMS activation
Catalytic chlorination
Marine pollutant control

ABSTRACT

Antibiotics (or pharmaceuticals) and inorganic nitrogen may coexist in mariculture wastewater, adversely affecting food safety and coastal ecology. Advanced treatment of marine wastewater is of great significance. In this study, simultaneous removal of refractory berberine chloride (BC) and ammonium nitrogen (NH_4^+-N) was firstly achieved in a visible-light-driven marine photocatalytic fuel cell/peroxymonosulfate (PFC/PMS) system. The modified blue TiO_2 nanotube arrays (TNA) anode and Cu-Co-WO_3 cathode bridged photo-electrocatalysis, sulfate radical-based oxidation and catalytic chlorination, benefiting both pollutant removal and fuel cell electricity generation. Under optimized conditions (double photoelectrodes, 2.5 mM PMS, R = 500 Ω), the system had an open circuit voltage of 0.57 V, removing 95% of BC and NH_4^+-N, meeting the discharge standard of mariculture. Natural-sourced COD_{Mn}, and inorganic nitrogen in simulated mariculture wastewater were also efficiently removed with power generation. The mechanism involving (photo-)electrocatalytic chlorination and PMS-chlorination theoretically supports the application/optimization of integrated electrochemical technologies for marine pollution control.

1. Introduction

Pharmaceuticals, including antibiotics, have been widely used in aquaculture to promote fish growth and prevent/treat infections [1]. However, their frequent use may promote bacterial resistance and consequently impact the infectious disease control and endanger human food safety. Although the usage of antibiotics has been strictly restricted in actual production, various residuals (including sulfonamides, fluoroquinolones, macrolides, chloramphenicols, etc.) were still detected in the seawater of maricultural area [2].

To reduce the reliance of aquacultural production to antibiotics, some low price and low toxic Chinese herb medicines, including berberine, were adopted [3]. As a natural isoquinoline alkaloid, berberine can not only kill pathogenic bacteria to prevent several fish diseases, but also have pharmacological effects such as enhancing fish immune response, improving antioxidative capacity, as well as reducing liver lipid accumulation, plasma total cholesterol and triglyceride [4]. Its most commonly used form is berberine chloride (BC) [5]. However, the wide use of this pharmaceutical in mariculture also poses a potential risk to seawater. At present, researches focusing on the treatment of berberine or other antibiotics in seawater are still limited [6]. Efficient treatment of such refractory organic pollutants in natural seawater, as well as the simultaneous removal of inorganic nitrogen, is of great significance for the sustainable development of mariculture.

Up to now, comprehensive treatment of mariculture wastewater focusing on organic pollutant control usually realized in biological systems which are high-efficiency and low-cost [7–10]. But in some circumstances when the chemical oxygen demand (COD) in low level is mainly derived from pharmaceuticals (such as the wastewater in breeding stage or recirculating system [11]), applications of these

* Corresponding author at: Key Laboratory of Industrial Ecology and Environmental Engineering (MOE), School of Ocean Science and Technology, Dalian University of Technology, 124221 Dalian, Liaoning, China.
E-mail address: lifenliu@dlut.edu.cn (L. Liu).

https://doi.org/10.1016/j.apcatb.2022.121215
Received 14 November 2021; Received in revised form 17 January 2022; Accepted 12 February 2022
Available online 16 February 2022

bio-based technologies are limited due to the insufficient carbon source, inappropriate carbon to nitrogen ratio and the potential risk of antibiotic resistance genes [12,13]. Comparatively, electrochemical technology is much suitable for advanced treatment of such kind of wastewater.

Taking advantages of intrinsic chloride ions (Cl^-) in natural seawater, electrochemical systems can easily trigger electrochemical chlorination for efficient marine pollutant control. This technology has been reported in various saline wastewater treatment, including the removal of antibiotics, conventional COD, ammonium and nitrous nitrogen, etc. [14–16]. However, the intense electric field and expensive electrode materials (mainly boron-doped diamond electrode (BDD) and RuO_2- or IrO_2-based dimensionally stable anode (DSA)) make it unsatisfactory in energy consumption, by-product generation and operating cost [17–19].

Integrating with other advanced oxidation processes (AOPs), such as photocatalysis, electrocatalysis, Fenton- and peroxymonosulfate (PMS)-based processes, is an effective strategy to enhance the oxidation capacities of electrochemical systems [20–23]. With the expansion and synergy of generating pathways of active species, more pollutants can be degraded in integrated electrochemical systems with lower electric field intensity. Thus, the by-product generation can be reduced, while the degradation becomes more efficient and complete. However, under the hindrance of background constituents in natural seawater, integration of multiple oxidative mechanisms in novel electrochemical systems still needs exploration, and the interactions among different pollutants/active species deserve in-depth study.

To construct an integrated electrochemical system, electrodes are essential in bridging different processes. Effective modification of electrodes for better catalytic performance can optimize the system in both pollutant removal efficiency and energy-savings. However, except the technical difficulty in loading powder-like catalyst, the modification of electrodes for higher-efficiency marine pollutant control are confronted with decline of activities, since most of the catalytic materials may be salt-deactivated in marine environment due to the impact of massive ions and impurities to their intrinsic structure, electron transport and mass transfer [24]. In addition, the metal (such as Cu, Fe, Ni, etc.) electrodes may become corroded in seawater. Thus, cost-effective electrodes with high catalytic performance and stable chemical properties in saline (marine) environment are urgently needed.

In this study, an integrated photocatalytic fuel cell (PFC)/PMS system was firstly constructed with optimized Cu-Co-WO_3 catalytic cathode and blue TiO_2 nanotube arrays (TNA) anode for marine pollutant control. With the assistance of visible light and proper amount of PMS, refractory organic pollutant (represented by BC) and inorganic nitrogen (ammonium nitrogen (NH_4^+-N)) can be simultaneously removed via integrated (photo-)electrocatalytic chlorination and PMS-chlorination. The comparison of system mechanism in freshwater and seawater revealed significant role of excessive Cl^- in changing pollutant oxidation pathways, which explained the inherent technical bottlenecks of traditional advanced oxidation technologies in saline (marine) wastewater treatment. This study provides a sustainable alternative for advanced removal of marine pollutants.

2. Materials and methods

All the chemicals were directly used after bought without further purification. Natural seawater (35‰ salinity with ~25,000 mg L^{-1} Cl^-) was obtained from Yellow Sea (Dalian, China).

2.1. Preparation of catalytic electrodes

2.1.1. Cu-Co-WO_3 cathode

(a) Preparation of Cu-Co-WO_3 catalyst

The powder-like catalyst of Cu-Co-WO_3 was simply prepared by one-step doping under microwave irradiation. Specifically, 0.01 mol of tungstic acid (H_2WO_4) was dissolved in 10 mL 1 M sodium hydroxide (NaOH) solution under continuous stirring. After hydrolyzing for 30 min, copper nitrate trihydrate ($Cu(NO_3)_2.3\ H_2O$) and cobalt nitrate hexahydrate ($Co(NO_3)_2.6\ H_2O$) were added at the molar ratio of W:CuCo = 1:1:1. After thoroughly dissolution, hydrochloric acid (HCl, 37 wt%) was dropwisely added to the solution under vigorous stirring, adjusting the pH to 1.0. Then the mixture was transferred into a Teflon reactor with the same amount of pure water (for microwave response), sealed and heated under 750 W microwave for 5 min. After naturally cooling down, the precipitate was washed by deionized water for several times, dried in air and ground for use. To compare the modification effect of elements doping, pure tungsten trioxide (WO_3) was also prepared by the same method without the introduction of Cu and Co elements.

(b) Preparation of Cu-Co-WO_3 catalytic electrode

The catalytic electrode was prepared by loading the powder-like Cu-Co-WO_3 on carbon fiber cloth (240 g m^{-2}, Yixing, China) via a modified phase-inversion method [25]. Casting solution consisted of 9.0 wt% of the catalyst, 4.0 wt% of polyvinylidene fluoride (PVDF), 3.0 wt% of polyvinylpyrrolidone (PVP), 3.0 wt% of carbon nanofiber (OD 150–200 nm, length 10–30 μm, Beijing DK nano technology Co., Ltd., China) and 81.0 wt% of N,N-dimethylformamide (DMF). For comparison, the thicknesses of the catalytic layer, controlled by an adjustable blade, were set as 100, 150, 200 and 300 μm, respectively.

2.1.2. Blue TiO_2 nanotube arrays (TNA) anode

The blue TNA electrode was prepared by a reported electrochemical method [26] which includes two-step anodization and one-step cathodic reduction of titanium sheet (4.0 × 5.0 cm^2, 0.3 mm thick). The constant current/voltage was supplied by an adjusted direct current regulated power supply (DP6010, Mestek electronics Co., Ltd).

2.2. Characterization of Cu-Co-WO_3 catalysts and catalytic electrodes

The optical performances of the catalysts were investigated by ultraviolet-visible spectrophotometer (UV-Vis, JASCO Corp., V-550). According to the UV-Vis diffuse reflectance spectrum, the optical band gaps were calculated by the equation of Tauc model [27]:

$$(\alpha h\nu)^n = A(h\nu - E_g) \quad (1)$$

Where α is absorption coefficient, $h\nu$ is the photon energy, n is equal to 1/2 for the analysis of WO_3 (indirect transition) and its composites in this case [28,29], A is a materials parameter and E_g is the bandgap energy.

Morphology of the catalysts and catalytic electrodes were characterized by high-resolution transmission electron microscope (TEM, JEM-F200, Japan) and scanning electron microscopy (SEM, SU5000, Japan) equipped with energy dispersive X-ray spectrometer (EDS, Ultim Max, UK). Structural information of the catalysts and electrodes was supplied by X-ray diffraction (XRD, SmartLab 9 kW, Japan) and X-ray photoelectron spectroscopy (XPS, K-Alpha+, USA).

Electrochemical performances of the as-prepared electrodes were tested by electrochemical workstation (CHI660E) in a three-electrode system with the counter electrode of platinum sheet (1.0 × 1.0 cm^2) and the reference electrode of saturated calomel electrode (SCE). Cyclic voltammetry (CV) test was conducted in the electrolyte of 5 mM $K_3[Fe(CN)_6]$ + 1 M NaCl at a scan rate of 50 mV s^{-1}. Electrochemical impedance spectroscopy (EIS) was tested in 1 M NaCl solution at 0 V (vs. SCE) potential from 0.1 to 10^5 Hz. The photo-current (I-t curve) of the anode was tested in 0.5 M Na_2SO_4 solution by applying intermittent illumination (Xenon lamp, PLS-SXE300D, Beijing Perfectlight Technology Co., Ltd., China) every 30 s to the working electrode. The apparent resistance (in average) of the catalytic electrode was obtained from 25

random points on the surface of catalytic layer by a multimeter (VC9800, Win Technology Co., Ltd., China).

2.3. Catalytic performance test of catalysts

The photocatalytic performance of the powder-like catalysts in PMS activation was compared in BC removal in fresh-water environment. Typically, 0.1 g L^{-1} catalysts were dispersed in 100 mL 20 mg L^{-1} BC solution under continuous stirring. After 30 min adsorption in dark, visible light was supplied to the system by a halogen lamp (50 W) suspended 7.0 cm above the reactor. PMS was optionally added at 0.5 mM. During catalytic degradation, absorbances of the water samples (taken at certain time intervals), were immediately tested at 343 nm by an ultraviolet-visible spectrophotometer (UV-5500, METASH, Shanghai) after filtrated by 0.22 μm membranes. The concentration of BC was calculated from the standard curve of $y = (x - 0.014)/0.0542$ ($R^2 = 0.999$), where x refers to the absorbance of water sample and y refers to the BC concentration (mg L^{-1}).

2.4. Construction of marine PFC/PMS system

A single chamber PFC was constructed with the as-prepared Cu-Co-WO_3 cathode (4.0 × 5.0 cm^2) and the blue TNA anode, which were connected through external resistance at an electrode spacing of 2.5 cm. Natural seawater containing 10 mg L^{-1} BC and/or 10 mg L^{-1} NH_4^+-N served as the electrolyte at a volume of 400 mL. Halogen lamps (50 W) were set for both of the electrodes to supply visible light irradiation. The distance between light source and electrode was 5.0 cm. Every time before experiment, the electrodes were immersed into the electrolyte at open circuit for 30 min to remove the physical adsorption. After that, catalytic degradation was started with 0.6 L min^{-1} aeration at controlled operating conditions in external circuit (opened/connected), external resistances, PMS concentrations and light irradiation. The configuration of the system was exhibited in Fig. A.1.

Water samples were taken at certain time intervals for analysis. Typically, the concentration of BC was characterized by spectrophotometry as the method in Section 2.3. The contents of nitrogen, chloramines (N, N-diethyl-phenylenediamine method) and COD_{Mn} were analyzed according to Chinese N.E.P.A. standard [30] and National Standards of the People's Republic of China (GB17378.4–2007). The power generation of the system was monitored by the multimeter and the power density (mW m^{-3} or mW m^{-2}) was calculated by U × I × 1000/C, where U (V) and I (A) are the cell voltage and current of the PFC system respectively, and C is the volume of the treated wastewater (m^3) or the effective area of the electrode (m^2).

2.5. Mechanism investigation

Free radical quenching experiment was conducted in optimized PFC/PMS system with different quenchers, which can eliminate specific active species before they react with pollutants. To support mechanism explanation, free radicals in the system (without pollutants) were also trapped by 50 mM 5, 5-dimethyl-1-pyrroline N-oxide (DMPO, Aladdin) or 10 mM 2, 2, 6,6-tetramethylpiperidine (TEMP, Aladdin) and detected by electron paramagnetic resonance (EPR, A200–9.5/12, Germany).

3. Results and discussion

3.1. Characterization of the Cu-Co-WO_3 catalyst and catalytic cathode

To endow the cathode with both photo-electrocatalytic performance and PMS-activating function, WO_3, with the advantages of economic cost, well chemical stability and great potential in visible-light response [31], was firstly modified by metallic components of Cu and Co via one-step doping, serving as the catalytic component of the carbon-based electrode. The loading amount of the catalyst related with the thickness of catalytic layer was further optimized.

3.1.1. Catalytic performance of Cu-Co-WO_3

As shown in Fig. 1(a), pure WO_3 only presented weak response in visible light region, while the doping of Cu and Co significantly enhanced its light absorbance, especially in the wavelength range of 420–650 nm. The bandgap energy was narrowed from 2.45 eV of WO_3 to 1.41 eV of Cu-Co-WO_3, confirming the enhanced the visible-light harvesting capacity and charge carrier generation after modification [32].

By using the target pollutant of BC, performance of the catalyst in photocatalytic PMS activation was tested. According to Fig. 1(b), 0.1 g L^{-1} Cu-Co-WO_3 can effectively activate 0.5 mM PMS to removal over 80% of BC (20 mg L^{-1}) in 20 min and 87.70% in 60 min, even without light irradiation. After supplying visible light, the removal rate was further enhanced to 96.19% (in 60 min), more than four times higher than that of pure WO_3 (Fig. 1(c)). Thus, this modified catalyst can not only intrinsically activate PMS by the doped Cu and Co, but also utilize visible light to assist refractory organic pollutant removal.

3.1.2. Structural and morphological analysis of the Cu-Co-WO_3 and the electrode

The as-prepared catalysts were characterized by XRD to identify their crystal structure. According to Fig. 2(a), hexagonal WO_3 was successfully synthesized by the one-step microwave method even without further calcination. The main peaks matched well with the standard spectrum of WO_3 in PDF#75–2187 (7.298 × 7.298 × 3.899, $\alpha = \beta = 90°$, $\gamma = 120°$). However, after doping with Cu and Co, the crystalline structure of WO_3 changed into triclinic phase (PDF#71–0305, 7.309 × 7.522 × 7.678, $\alpha = 88.81°$, $\beta = 90.92°$, $\gamma = 90.93°$). The enlarged cell volume confirmed the successful insert of Cu and Co (with larger ion-radius than W) in the lattice of WO_3. The broader peaks with lower intensity indicated the reduced crystallinity of Cu-Co-WO_3 than pure WO_3, which may provide better performance with smaller particle size. However, no peak relates to Cu or Co was detected in the pattern of Cu-Co-WO_3 due to the tiny doping amount. Their existence was evinced by XPS and EDS characterization in the following discussion.

The detailed structural information of the Cu-Co-WO_3 was provided by XPS analyzation. Specifically, in the survey spectrum of Fig. 2(b), all the elements, including trace amount of Cu and Co, were detected. The relative atomic ratio of Cu/Co (~ 1.3) corresponds well with the EDS result in Fig. A.2 where the doping amounts of Cu and Co were determined as 2.85 at% and 1.56 at%, respectively. Elemental status of Cu-Co-WO_3 was investigated by high-resolution spectra (Fig. 2(c)-(f)). W 4 f presented doublet-line spectrum with two peaks of W 4 $f_{5/2}$ and W 4 $f_{7/2}$ at 38.0 and 35.9 eV, respectively, matching well with the W^{6+} of WO_3 in both peak position and spacing [33,34]. The deconvoluted peaks of O 1 s at 530.7 and 531.3 eV referred the oxygen in structure of the sample with some absorbed hydroxide (−OH) [33]. The doped Cu 2p had disassembled peaks at 932.8 eV (Cu $2p_{3/2}$) and 952.7 eV (Cu $2p_{1/2}$), confirming the existence of Cu^+ in the form of Cu_2O. Meanwhile, the split peaks at 935.2 (Cu $2p_{3/2}$), 955.0 (Cu $2p_{1/2}$), 941.0 and 943.8 eV (shake-up satellites) demonstrated the coexistence of Cu^{2+} [33]. In the spectrum of Co 2p, peaks at 782.1 and 797.6 eV, with the satellite peaks at 787.8 and 803.7 eV, were assigned to Co $2p_{3/2}$ and Co $2p_{1/2}$, respectively. The split peaks confirmed the existence of Co^{2+} (781.5 and 797.3 eV) and Co^{3+} (782.4 and 797.8 eV) in the form of Co_3O_4 [35,36].

By loading the Cu-Co-WO_3 on carbon fiber cloth, catalytic electrode was prepared. The morphology of the modified electrode (with 200 μm-thick catalytic layer) was observed by SEM. According to Fig. 3(a) and (b), the electrode had smooth surface with porous layer in microstructure, which benefited the contact of the catalytic component in solid phase and the pollutants in water phase. The micron pores may also endow the electrode with filtration potential in some applications. In EDS mapping results (Fig. 3(c)), all the elements in the Cu-Co-WO_3 were detected on the surface of the electrode, together with the C and F in

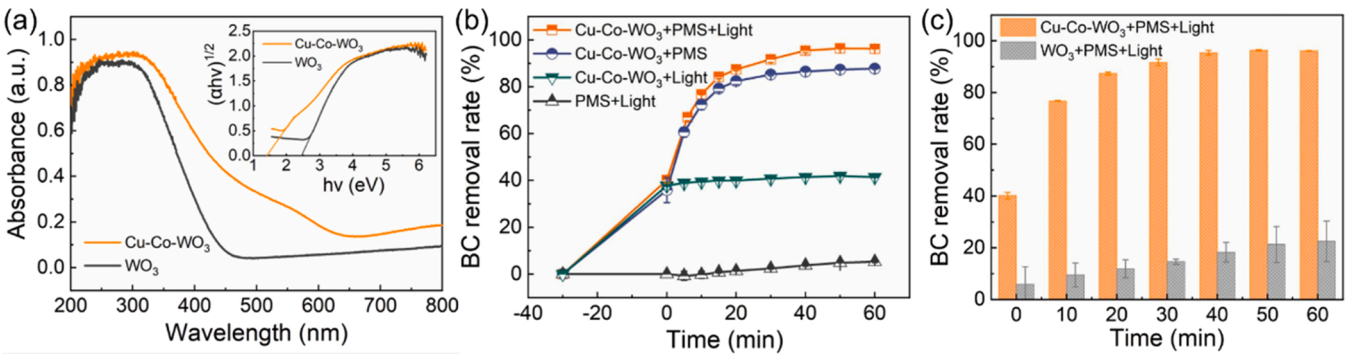

Fig. 1. (a) UV-Vis diffuse reflectance spectrum and Tauc plots (insert) of Cu-Co-WO_3 and WO_3. (b) BC removal rates of Cu-Co-WO_3 under different conditions. (c) BC removal rates of Cu-Co-WO_3 and WO_3 with PMS under visible light irradiation. ([Catalyst] = 0.1 g L^{-1}, [BC] = 20 mg L^{-1} in deionized water, [PMS] = 0.5 mM).

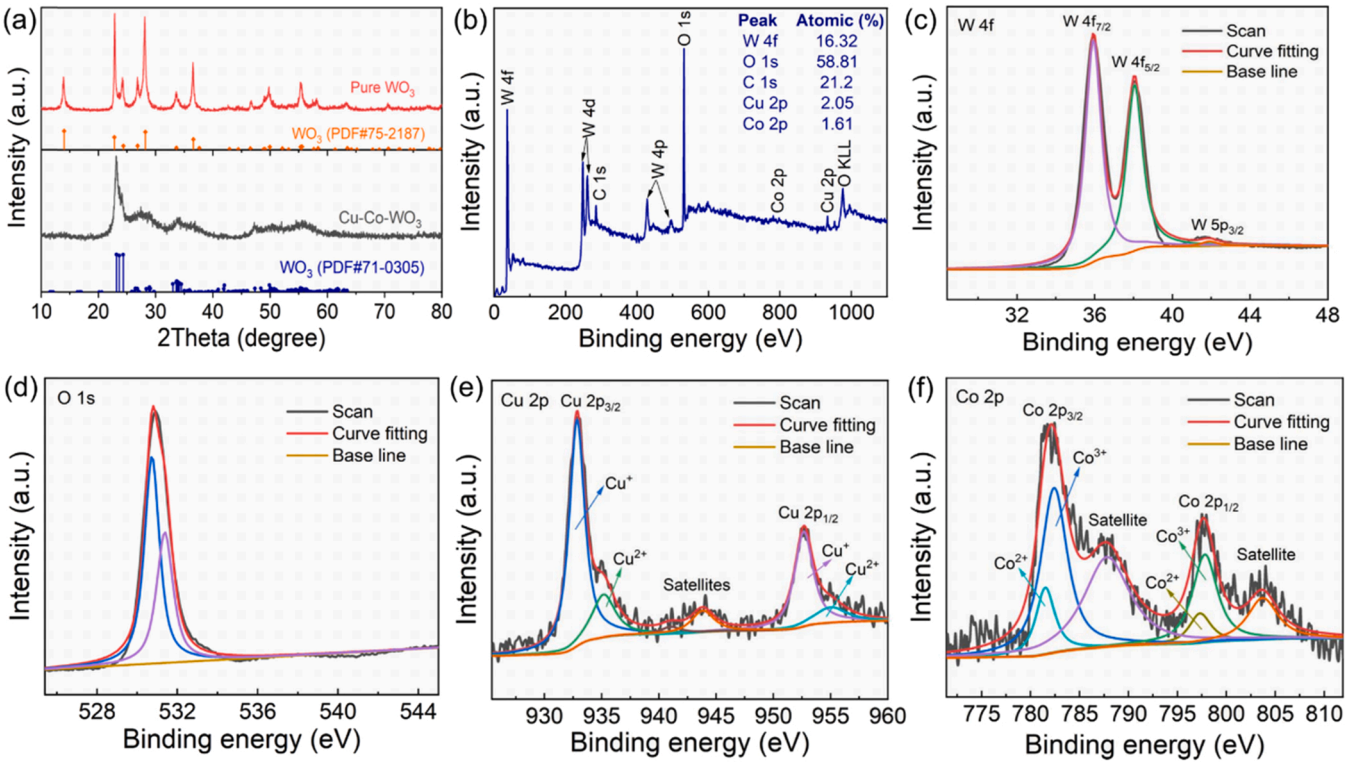

Fig. 2. (a) XRD spectra of WO_3 and Cu-Co-WO_3. (b) XPS survey spectrum of Cu-Co-WO_3. High-resolution spectra of (c) W 4 f, (d) O 1 s, (e) Cu 2p and (f) Co 2p in Cu-Co-WO_3.

structure, confirming the successful loading of this agglomerated nano-needle catalyst. The even distribution of Cu-Co-WO_3 may endow the electrode with excellent photo-assisted PMS activating performance.

3.1.3. *Electrochemical performance of the Cu-Co-WO_3 electrode*

Electrochemical performance of the Cu-Co-WO_3 electrodes with different thicknesses of catalytic layer was compared. According to the CV curves in Fig. 4(a), the loading of Cu-Co-WO_3 effectively enhanced the catalytic activity of carbon fiber cloth. But the promotion gradually weakened with the increasing thickness of catalytic layer, although the "300 μm" sample had slightly higher redox peaks than the other samples due to the high loading amount of the catalyst. In the EIS test, as shown in Fig. 4(b), Nyquist plots of the series of electrodes are in arc shape. The smaller the arc radius, the lower the charge transfer resistance (R_{ct}) of the electrode [37]. Combining with the fitting results in Table 1, the loading of Cu-Co-WO_3 effectively decreased the R_{ct} of the carbon-based electrode. The thickness of catalytic layer positively influenced the charge transfer efficiency of the electrode by increasing the loading amount of the catalyst. However, when the thickness increased over 200 μm, further decrease of R_{ct} was neglectable due to the inefficient contact of surface catalyst with electrode substrate. Since the electrode with 200 μm-thick catalytic layer presented the lowest total ohmic resistance (R_s + R_{ct}) of 2.85 Ω·cm^2, it was chosen as cathode in the following experiments, comprehensively considering the conductivity/resistance/reactivity of the electrode and the usage of the catalyst. The apparent conductivity of the optimized electrode was tested to be 1.00×10^{-2} S cm^{-1}.

3.2. *Characterization of the blue TNA photo-anode*

Morphology of the blue TNA electrode was observed by SEM. As shown in Fig. 3(d) and (e), well-arranged nano tubes with the diameter of around 60 nm formed a dense film on the surface of the electrode. The elemental composition of the blue TNA was assigned to be Ti and O

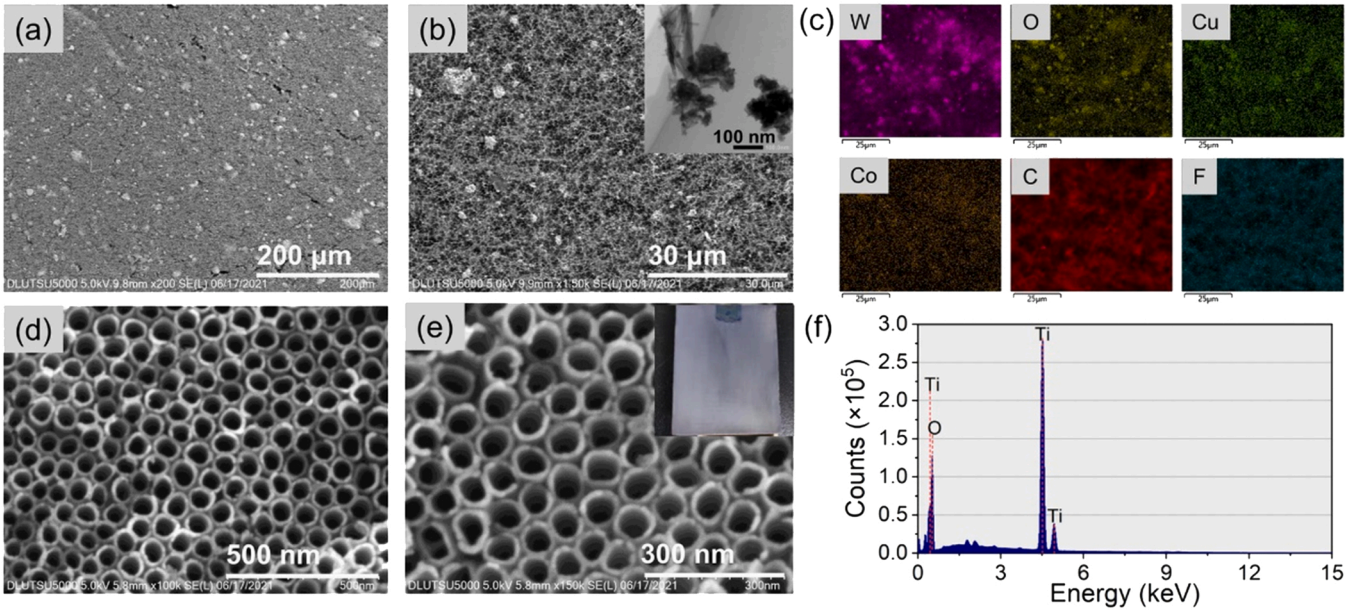

Fig. 3. (a) and (b) SEM images of Cu-Co-WO_3 electrode and the catalyst (insert). (c) EDS mapping results of Cu-Co-WO_3 electrode. (d) and (e) SEM images of blue TNA electrode and its physical picture (insert). (f) EDS results of blue TNA electrode.

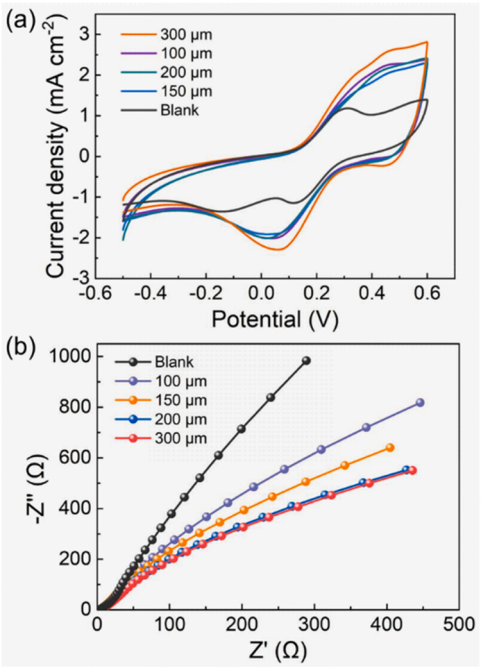

Fig. 4. (a) CV and (b) EIS curves of Cu-Co-WO_3 electrodes with different thicknesses of catalytic layer.

Table 1
EIS fitting results (ohmic resistance) of the modified electrodes with different thicknesses of catalytic layer.

Thickness of the catalytic layer	R_s ($\Omega \cdot cm^2$)	R_{ct} ($\Omega \cdot cm^2$)	Equivalent circuit
Blank	3.74	3.08×10^{13}	
100 μm	3.80	4.87	
150 μm	3.78	0.083	
200 μm	2.83	0.0161	
300 μm	3.26	0.0103	

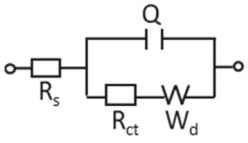

according to Figs. 3(f) and 5(a). The crystalline phase of the electrode was identified by XRD as the mixture of TiO_2 (PDF#21–1272) and Ti_3O_5 (PDF#82–1138) (Fig. 5(b)), due to the combined electrochemical oxidation and reduction processes. The sharp peaks of XRD pattern indicate its well crystallization. To further confirm the valence status of Ti and O, high-resolution spectra were analyzed in Fig. 5(c) and (d). For Ti 2p, characteristic peaks of both Ti^{3+} (at 464.8 eV for Ti $2p_{1/2}$ and 458.9 eV for Ti $2p_{3/2}$) and Ti^{4+} (at 463.9 eV for Ti $2p_{1/2}$ and 458.4 eV for Ti $2p_{3/2}$) were observed, indicating the successful modification of TNA [14,38]. Ti^{3+} formed in electrochemical reduction process promised the excellent photo-electrochemical performance of the electrode in visible light region [26,39]. The spectrum of O 1 s, with the peaks at 531.9, 530.3 and 529.8 eV belonging to oxygen vacancies, absorbed -OH on the surface and Ti-O in the structure respectively, further confirmed the formation of blue TNA after electrochemical modification [39].

The photo-electrical performance of the blue TNA electrode was evaluated by I-t curve in Fig. 5(e). With intermittent irradiation of simulated sunlight, the modified electrode presented much higher and more stable photocurrent output than the unmodified titanium sheet. The excellent photo-electric conversion efficiency should be attributed to the reductive Ti^{3+} which modified the band structure of TiO_2. This blue TNA electrode was supposed to serve as the anode of PFC to support photo-electric field.

3.3. Optimization of PFC/PMS system in marine organic pollutant removal

With the as-prepared Cu-Co-WO_3 catalytic cathode and blue TNA anode, a visible-light PFC system was constructed, aiming at marine organic pollutant removal. By using BC as the target pollutant, the type of electrodes, external resistance and other operating conditions including light irradiation and PMS addition were comparatively studied.

The performances of Cu-Co-WO_3 cathodes with different thicknesses of catalytic layer were compared in PFC/PMS system with the blue TNA anode and 2000 Ω external resistance. As shown in Fig. 6(a), the loading of Cu-Co-WO_3 effectively enhanced the BC removal rate in natural seawater with the assistance of visible light irradiation and 0.5 mM PMS. The electricity generation of the double-photoelectrode system was also enhanced from 0.20 V with unmodified cathode (blank) to

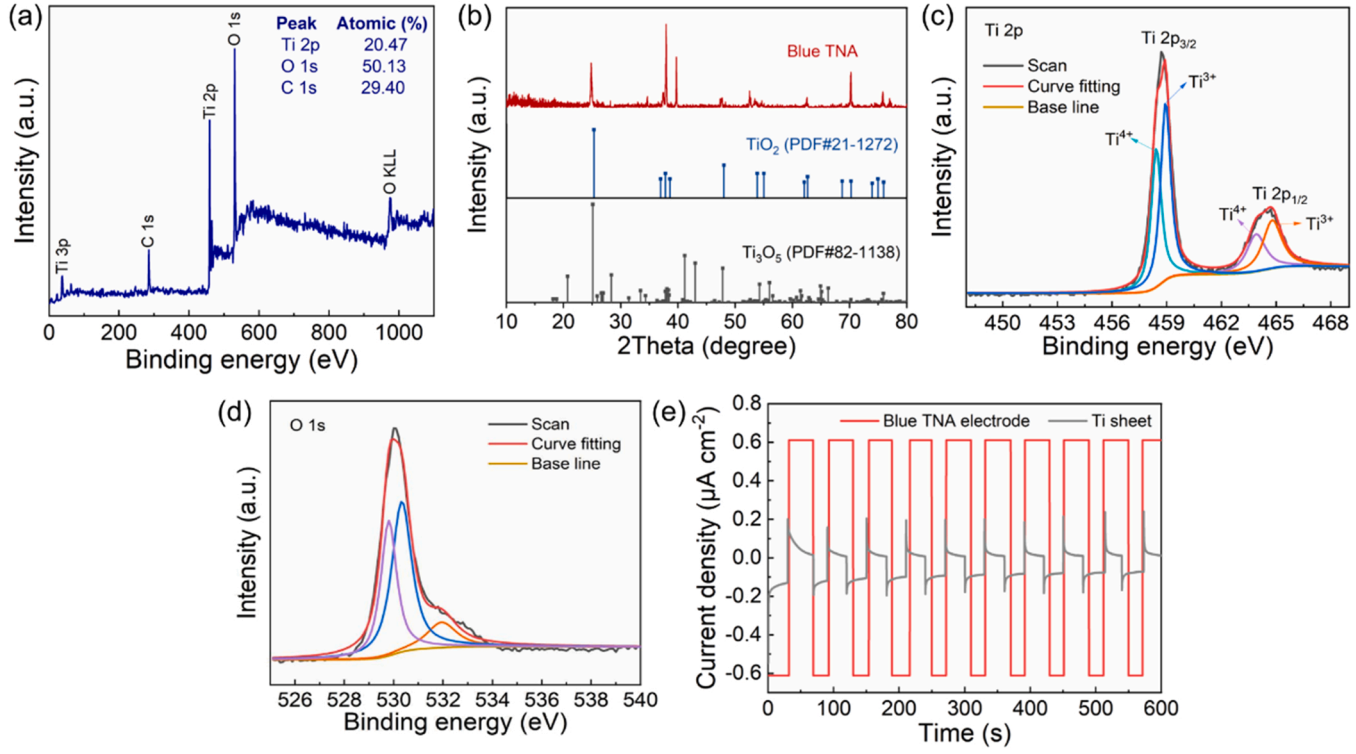

Fig. 5. (a) XPS survey spectrum and (b) XRD spectrum of the blue TNA electrode. High-resolution spectra of (c) Ti 2p and (d) O 1 s in blue TNA electrode. (e) I-t curves of the blue TNA electrode and titanium sheet.

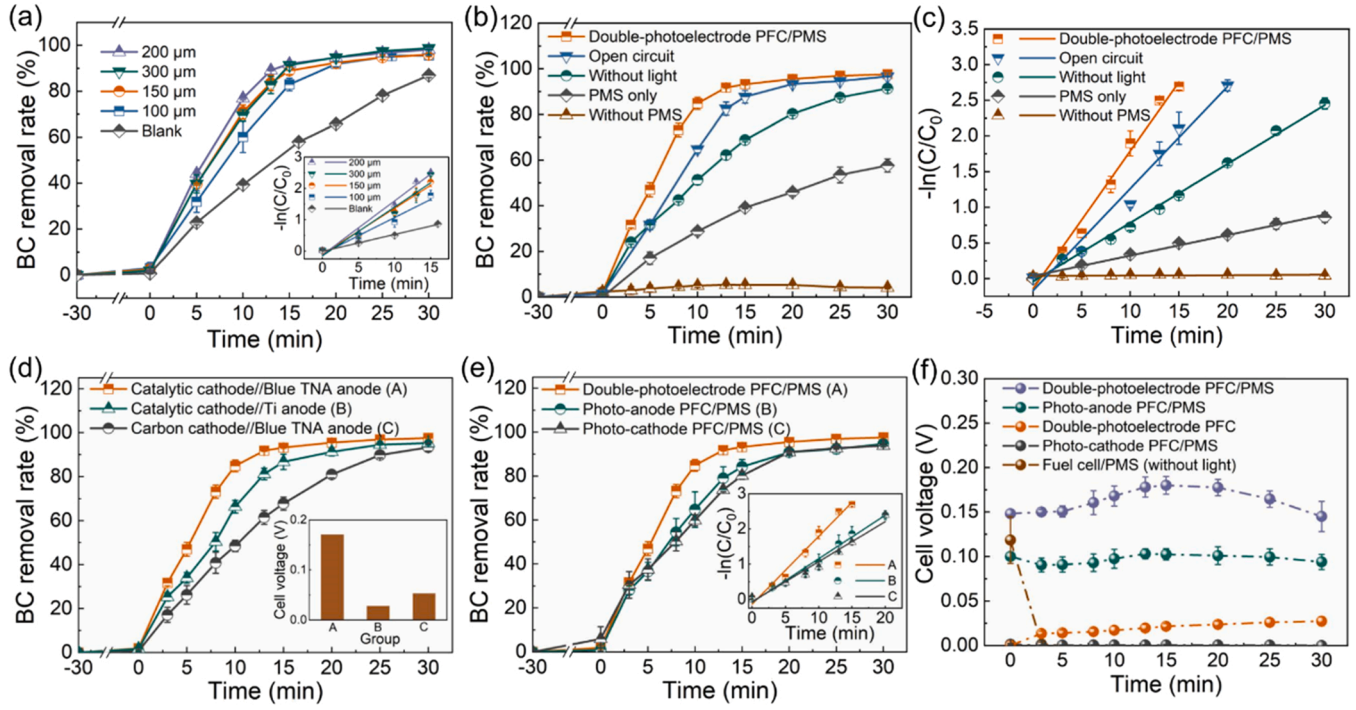

Fig. 6. (a) BC removal rates and efficiencies (insert) of the marine PFC/PMS system (double photoelectrodes) with different thicknesses of Cu-Co-WO_3 cathode. (b) BC removal rates and (c) efficiencies of the marine PFC/PMS system (double photoelectrodes) under different operation conditions. (d) BC removal rates and efficiencies (insert) of the marine PFC/PMS system (double photoelectrodes) with different electrodes (e) BC removal rates and efficiencies (insert) of the marine PFC/PMS system with different illuminating conditions. (f) Power generation of the marine PFC/PMS system under different operating conditions. ([BC] = 10 mg L^{-1} in natural seawater, [PMS] = 0.5 mM, R = 500 Ω).

around 0.42 V with catalytic cathodes, confirming the efficient modification of the carbon-based cathode in both photo-electrochemical performance and PMS activation. The thickness of catalytic layer mainly influenced the system performance in pollutant removal efficiency, resulting in the sequenced reaction rate constants of 200 μm > 300 μm > 150 μm > 100 μm > blank, which corresponded well with the EIS results (Section 3.1.3). Therefore, the resistance of the cathode affected the oxidation efficiency of the marine PFC/PMS system. The electrode with 200 μm-thick catalytic layer can better balance the charge-transfer and catalytic efficiencies.

By using the optimized catalytic cathode (200 μm), the influence of external resistance on the performance of marine PFC/PMS system was further investigated. As shown in Table 2 and Fig. A.3, more than 93% of the BC can be effectively removed in 20 min at all external resistances, which should be attributed to the strong effect of the integrated photocatalysis, PMS oxidation and chlorination, rather than electrochemically dominated process. However, in the aspect of system power generation, the resistance played a leading role. According to Table 2, the cell voltage increased with the external resistance until reached 0.57 V at open circuit, which is competitive even comparing with microbial fuel cells in marine environment [40]. Although the increase of external resistance can promote electricity output, it also decreased the current of the system for redox reactions. The highest reaction rate constant of this marine PFC/PMS system presented at 500 Ω, where more than 90% of BC can be degraded within 13 min with 0.17 V voltage output. The power generation of this optimized system in marine BC removal was 146.02 mW m^{-3} (or 29.20 mW m^{-2}).

To clarify the roles of electrodes, electric filed, light irradiation and PMS played in this integrated PFC/PMS system for marine pollutant control, comparative experiments were conducted and the test conditions were optimized. As shown in Fig. 6(b) and (c), the system had superior BC degradation efficiency with double photoelectrodes and 0.5 mM PMS, at which circumstance 97.55% was removed in 30 min with 91.77% in the first 13 min. The absence of PMS, light irradiation and electric field (open circuit) decreased the BC removal efficiency (rate constant) by 343.42, 2.35 and 1.35 times, respectively, indicating the synergistic effect of photo-electrocatalysis and PMS in advanced oxidation of this marine system, where the latter one played the leading role. Moreover, comparing the control groups of "without light" (with electrodes) and "PMS only" (without electrode), the modified electrodes (mainly the Cu-Co-WO_3 cathode) brought a 33.76% enhancement in BC removal (in 30 min) even without light irradiation. Thus, the modified electrodes well bridged the photo-electrochemical catalysis and PMS activation in natural seawater, helping improve oxidation capacity of the marine PFC/PMS system.

To demonstrate the function of the modified electrodes at optimal system conditions (double photoelectrodes and 500 Ω external resistance), BC removal was also measured with unmodified anode or cathode. As shown in Fig. 6(d), the PFC/PMS system had efficient pollutant removal together with delighted power generation only with the blue TNA anode and Cu-Co-WO_3 cathode. Using unmodified titanium anode or bare carbon fiber cloth cathode led to significant decrease of pollutant removal efficiency and cell voltage. Moreover, as expected, the blue TNA anode mainly affected the power generation of the system while the Cu-Co-WO_3 cathode contributed more to the pollutant removal.

The influence of light illumination on the performance of the PFC/PMS system (500 Ω external resistance) was presented in Fig. 6(e), which further illustrated the function of the modified electrodes. Specifically, the system had superior performance in BC removal when supplying visible light to both of blue TAN anode and Cu-Co-WO_3 cathode than to only one electrode. In addition, the single photoelectrode PFC/PMS systems had similar performances, indicating the positive role of light intensity in promoting integrated catalysis. However, in the aspect of power generation, different function of the photoanode and the photo-cathode was shown. In Fig. 6(f), the system had voltage output only when the anode was illuminated. The cell voltage (in average, the same below) of PFC/PMS system with double photoelectrodes was 1.67 times higher than that without cathodic illumination, and was also 9.09 times higher than that without PMS addition. Therefore, the power generation of the system mainly depends on the excellent photo-electrochemical performance of the blue TNA anode, while the cathode and the PMS also played an indispensable role.

Through the above analysis, the operating conditions of this marine PFC/PMS system were optimized as double photoelectrodes of blue TNA anode and Cu-Co-WO_3 cathode (200 μm) with 500 Ω external resistance, under which highly efficient BC removal and considerable system power generation can be promised.

Table 2
Performance of the marine PFC/PMS system in BC removal at different external resistances.

External resistance	BC removal rate (%, in 20 min)	Reaction rate constant k (min^{-1})	R^2	Cell voltage (V)
Open circuit	93.33 ± 0.52	0.143 ± 0.011	0.970	0.568
2000 Ω	94.64 ± 0.09	0.172 ± 0.013	0.978	0.417
1000 Ω	94.25 ± 0.17	0.176 ± 0.013	0.969	0.281
500 Ω	95.48 ± 0.05	0.193 ± 0.011	0.981	0.171
200 Ω	95.41 ± 0.37	0.184 ± 0.011	0.980	0.071
100 Ω	94.69 ± 0.61	0.169 ± 0.014	0.962	0.037

3.4. Simultaneous removal of marine organic pollutant and ammonium nitrogen in integrated PFC/PMS system

Ammonium nitrogen commonly coexists with organic pollutant in mariculture wastewater. Simultaneous removal of BC and NH_4^+-N were tested in the optimized marine PFC/PMS system. With the coexisted 10 mg L^{-1} NH_4^+-N, BC removal in this system decreased from 97.55% (without NH_4^+-N) to 54.19% in 30 min (Fig. 7(a)), at the initial PMS concentration of 0.5 mM. The impact of NH_4^+-N to BC removal should be attributed to the competition of oxidative species between inorganic nitrogen and organic pollutants. Since the removal rates of both BC and NH_4^+-N (only 27.60%) were far from satisfaction, the amount of PMS should be increased to expand oxidative capacity of this system.

According to Fig. 7(a), the removal of BC as well as NH_4^+-N was enhanced with the increasing amount of PMS due to the increased oxidative species. When the initial PMS increased to 2.5 mM, both BC and NH_4^+-N removal rates reached around 95% in 30 min. The molar ratios of the removed pollutants and the consumed PMS were 29.34% for NH_4^+-N and 1.00% for BC (decreased from 5.35% at 0.5 mM PMS due to the coexistence of NH_4^+-N). The remained COD_{Mn} and NH_4^+-N were 3.24 and 0.46 mg L^{-1} respectively, below the discharge standard of mariculture (Chinese industry standard, SC/T 9103–2007). Although the cell voltage decreased to around 63 mV during treatment due to the coexistence of NH_4^+-N (affecting electron transmission process), the self-biased electric field can still support the integrated electrochemical process in this PFC system. Thus, for the treatment of minor-polluted mariculture wastewater (with initial NH_4^+-N of ~10 mg L^{-1} and COD_{Mn} of ~5 mg L^{-1} from conventional/refractory organic pollutants), 2.5 mM PMS was enough.

Under the optimized operating conditions (double photoelectrodes of blue TNA anode and Cu-Co-WO_3 cathode (200 μm), R = 500 Ω, PMS = 2.5 mM, the same below), the products after BC and NH_4^+-N removal were analyzed. In the full wavelength spectrum of water samples (Fig. 7(b)), all the characteristic peaks belonging to BC disappeared after treatment, indicating complete degradation of BC instead of converting to other intermediate products. The final products should be the H_2O and CO_2 with small amounts of NO_3^- [41]. The concentrations of other inorganic nitrogen including NO_3^--N and NO_2^--N were detected to ensure the oxidation products of NH_4^+-N. Typically, 10.28 mg L^{-1} NH_4^+-N was removed with only 1.24 mg L^{-1} NO_3^--N and tiny amount of NO_2^--N (< 0.012 mg L^{-1}) generation, revealing the high nitrogen

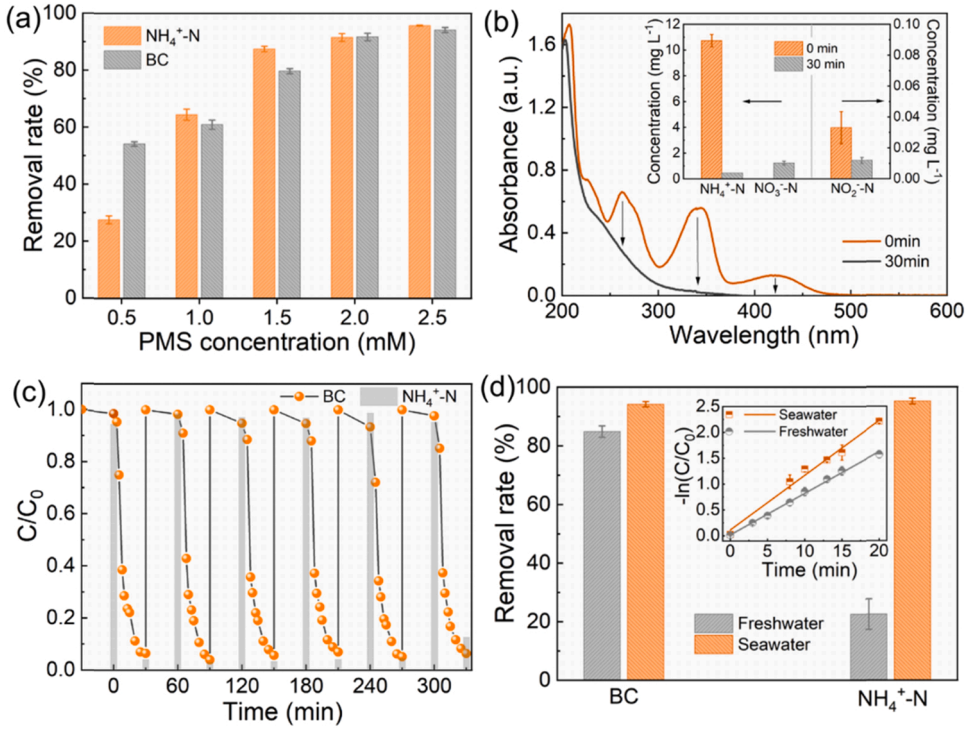

Fig. 7. (a) BC and NH_4^+-N removal rates of the marine PFC/PMS system with different concentrations of PMS. (b) Full wavelength spectrum of the treated seawater (under optimized conditions) and the remained inorganic nitrogen. (c) Reusability of the optimized marine PFC/PMS in BC and NH_4^+-N removal. (d) BC and NH_4^+-N removal rates and BC removal efficiencies (the insert) of the optimized PFC/PMS system in fresh-water and seawater environment.

selectivity of 88.13% (calculated by ΔN/ΔC, where ΔN and ΔC refer to the changes of molecular nitrogen and NH_4^+-N concentrations in 30 min, respectively). Moreover, the remained total chlorine was below 0.20 mg L^{-1}, including 0.082 mg L^{-1} free chlorine and almost undetected chloramines, meeting the discharge standard of mariculture (Chinese industry standard, SC/T 9103–2007). Thus, this PFC/PMS system can effectively remove organic pollutants and inorganic nitrogen from natural seawater by utilizing the self-generated electric field, which largely restricted the by-product generation comparing with externally charged electrochemical systems [14–16].

Reusability of the system was tested by repeating experiment where the electrodes were simply washed by deionized water after each cycle. According to Fig. 7(c), the optimized PFC/PMS system can effectively remove 94.82% of BC together with 95.63% of NH_4^+-N in natural seawater even in the fifth run, confirming the reusability of the electrodes/system. Slight decrease of removal rate was firstly observed in NH_4^+-N (to 87.33%) when further increased the reusing cycle. The prior degradation of BC than NH_4^+-N should be attributed to the strong oxidation effect of $^1O_2$ to organics (with carbon-carbon bonds) rather than inorganic nitrogen [42].

To explore the effect of marine environment on pollutant removal, tests in freshwater (tap-water) matrix was conducted in the optimized PFC/PMS system. According to Fig. 7(d), more than 70% of NH_4^+-N removal was inhibited in fresh-water environment comparing to that in seawater. The cell voltage of this system also decreased 34.9% to 40.97 mV due to the change of water conductivity. Comparatively, BC removal rate was less affected by the water environment since only 8.62% decline in freshwater was observed.

The decrease in performance of the system in non-saline (freshwater) environment than in natural seawater should be attributed to the absence of excessive Cl^-. Typically, natural seawater contains around 25000 mg L^{-1} of Cl^-, more than 1000 times higher than that of tap-water [43]. It can be concluded that excessive Cl^- in seawater naturally participated in the reactions among oxidative species besides with photo-electrocatalysis and PMS-advanced oxidation, affecting pollutant removal efficiency. The reactive chlorine species (RCS), which may form in this PFC/PMS system, compensated for the hindrance of background constituents in natural seawater and contributed to pollutant removal. The relatively high BC removal rate (84.85%) in freshwater revealed the easier degradation of organic pollutants via non-chlorine oxidative species such as •OH and SO_4•$^-$ etc. than that of inorganic nitrogen (NH_4^+-N) which mainly relies on the chlorine-mediated oxidation. The easy activation of Cl^- in this integrated PFC/PMS system made it especially suitable for marine pollutant control.

The insight mechanism of this marine PFC/PMS system was investigated by free radical quenching experiment. Specifically, quenchers (in Table 3) for sulfate radical (SO_4•$^-$), reactive oxygen species (ROS) and RCS were added to the system and the removal rates of BC and NH_4^+-N were detected (Fig. 8(a)).

SO_4•$^-$ and •OH were reported to be the main radicals in most of the PMS-based technologies [44,50,51]. However, in this marine PFC-PMS system, methanol (MeOH) and benzoic acid (BA) presented negligible influence on both BC and NH_4^+-N removal, indicating the unimportant role of •OH and SO_4•$^-$, together with Cl• and Cl_2•$^-$. Similarly, nitrobenzene (NB), a quencher for •OH in the presence of Cl•, also had little effect on pollutant oxidation (although BC cannot be detected), further confirming the low content of •OH. In addition, the role of •O_2^- was also ruled out from this system due to the similar performance of the marine PFC/PMS system under oxygen-containing (blank) and N_2-saturated conditions (exclude O_2 by N_2 aeration). Thus, the pollutant degradation mechanism in this marine PFC/PMS system was quite different from the traditional photocatalytic and/or PMS-based advanced oxidation.

Obvious inhibition of pollutant removal was observed in the system with 1,4-dimethoxybenzene (DMB) or tert-butyl-alcohol (TBA). Specifically, with 100 mg L^{-1} DMB, BC and NH_4^+-N removal rates in 30 min were decreased for 37.86% and 78.24%, respectively, illustrating the significant role of ClO•. Accordingly, TBA also decreased the NH_4^+-N removal rate for over 10% and retarded the BC removal in efficiency (Fig. 8(b)). Thus, Cl^- in natural seawater participated in pollutant oxidation of the PFC/PMS system mainly in the form of ClO•. The

Table 3
Reaction rate constants of different quenchers with specific radicals/species.

Quenchers	Reaction rate constants (M^{-1} s^{-1})						Ref.
	$SO_4\bullet^-$	•OH	$^1O_2$	Cl•	$Cl_2\bullet^-$	ClO•	
Methanol (MeOH)	2.5×10^7	9.7×10^8	–	1.0×10^9	–	–	[44,45]
Tert-butyl-alcohol (TBA)	–	6.0×10^8	–	3.0×10^8	–	1.3×10^7	[46]
1,4-dimethoxybenzene (DMB)	–	–	–	–	–	2.1×10^9	[47]
Benzoic acid (BA)	1.2×10^9	4.2×10^9	–	1.8×10^{10}	2.0×10^6	–	[45,47]
Nitrobenzene (NB)	–	3.9×10^9	–	–	–	–	[48]
L- histidine (L-his)	–	–	3.2×10^8	–	–	–	[49]

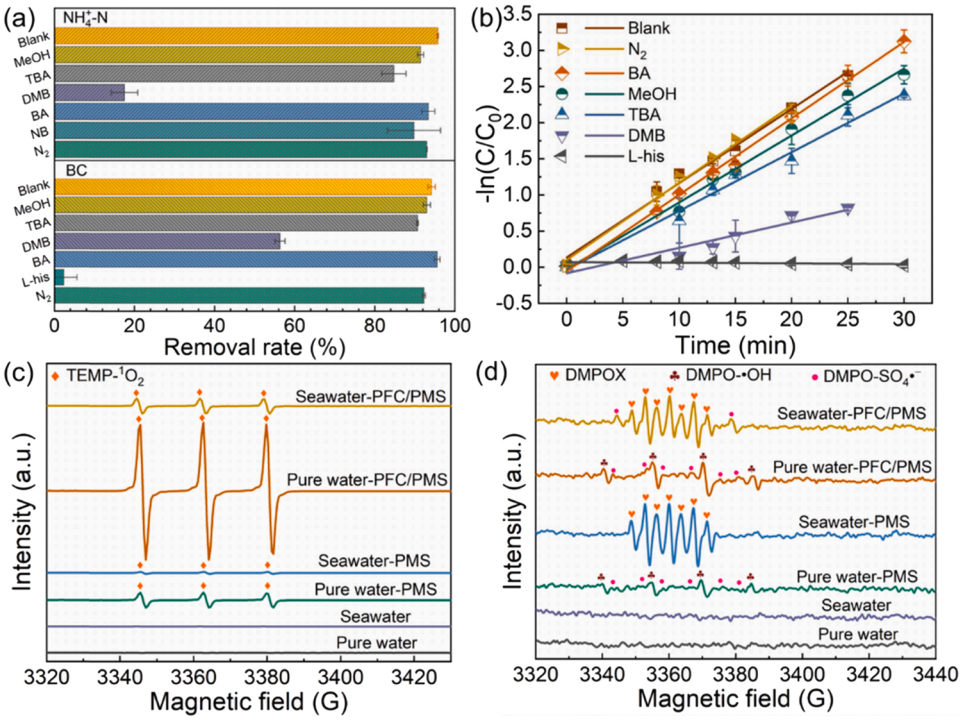

Fig. 8. (a) NH_4^+-N and BC removal rate (b) BC removal efficiency in free radical quenching experiment of the marine PFC-PMS system under optimized conditions (where MeOH, TBA, DMB, BA, NB and L-his refer to methanol, tert-butyl-alcohol, 1,4-dimethoxybenzene, benzoic acid, nitrobenzene and L-histidine at contents of 1 M, 1 M, 100 mg L^{-1}, 100 mg L^{-1}, 10 mM and 10 mM, respectively, "blank" refers to the experimental group without scavenger and "N_2" refers to the control group working in N_2-saturated condition). (c) and (d) EPR results of the system.

weakened role of •OH, $SO_4\bullet^-$ and Cl• in this system should be attributed to the rapid reactions among free radicals in the presence of Cl^-.

Among these scavengers, L-histidine (L-his), which can react with both PMS and $^1O_2$ [52], showed the greatest inhibition to the performance of PFC/PMS system. When adding 10 mM L-histidine to the system, BC was hardly removed, and the NH_4^+-N concentration reversely increased for around 50% after treatment, which should be attributed to the decomposition of amino groups in L-histidine itself under the attack of other strong oxidative species. Thus, $^1O_2$, related with PMS, was the main oxidative species (besides the chlorine related species) responsible for pollutant removal in this marine PFC-PMS system.

The existence of free radicals was further confirmed by EPR test in both sea-water and pure-water environment to clear the influence of Cl^- in radical generation. In Fig. 8(c), significant triplet signal of TEMP-$^1O_2$ was detected from the marine PFC/PMS system under optimized conditions, confirming the existence of $^1O_2$. The samples of "PFC/PMS" had stronger peaks than "PMS" in both seawater and pure water, illustrating the catalytic effect of the modified electrodes in PMS activation. However, comparing the patters of "PFC/PMS" (or "PMS") in seawater and pure water, the signal of $^1O_2$ was weakened in marine environment. Thus, the high concentration of Cl^- may promote the transformation among free radicals and decrease the generation of $^1O_2$ from PMS activation. Moreover, the formation of RCS also inhibited the photocatalytic generation of $O_2\bullet^-$ by the cathodic Cu-Co-WO_3 (Fig. A.4) [53], further resulting in the decrease of $^1O_2$. The lowered content of $^1O_2$ in natural seawater explained for the inevitable loss of oxidation capacity when applying PMS-based technology to marine pollutant control.

DMPO was used to trap free radicals including ROS, RCS and sulfate radical (Fig. 8(d)). As most of the reported PMS-based system, DMPO-•OH signal with the intensity ratio of 1:2:2:1 was observed with the concomitant peaks of DMPO-$SO_4\bullet^-$ in pure-water environment, indicating successful activation of PMS in this system. The stronger peaks of the sample "PFC/PMS" than "PMS" (in pure water) again confirmed the positive effect of the catalytic cathode in PMS activation. However, in marine environment, characteristic peaks of •OH and $SO_4\bullet^-$ were substituted/overlapped by seven-split peak with the intensity of 1:2:1:2:1:2:1, which was assigned to be 5,5-dimethy-2-pyrroline-N-oxyl (DMPOX). It is a nitroxide radical generated from direct oxidation of DMPO by strong oxidative (single electron) species, such as hypo-chloric acids/radicals and an immense amount of •OH suddenly generated at neutral pH [54–56]. Thus, marine environment greatly changes the oxidation pathway of pollutants, influencing the performance of traditional PFC or PMS systems in water treatment efficiency.

3.5. Mechanism explanation

Based on above analysis, an integrated mechanism involving radical and non-radical pathway was proposed for the marine PFC/PMS system, where $^1O_2$ and HClO/ClO^- played the dominant role (Scheme 1 (right)).

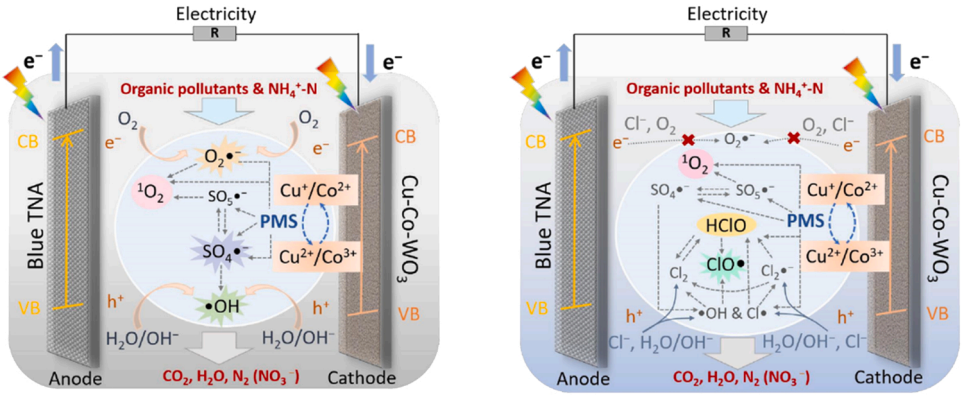

Scheme 1. Mechanisms of the PFC/PMS system in fresh-water environment (left) and marine environment (right).

The generation and interactions of oxidative species were exhibited in the following equations, including the photo-assisted PMS activation (Eqs. (2)-(13)) and photo-/PMS-catalytic chlorination (Eqs. (14)-(25)) [45,57–61]. For contrast, mechanism of the system working in fresh-water environment was also illustrated.

Specifically, the electrodes modified in optical performance can response to visible-light irradiation, generating electrons and holes for pollutant removal and constructing electric field for the PFC system via external circuit. Meanwhile, with additional PMS, an integrated mechanism of (photo-)catalytic PMS-advanced oxidation can be formed thanks to the cathodic catalytic material of Cu-Co-WO_3. The introduction of PMS in PFC not only extended pathways for free-radical generation, but also promoted charge transfer efficiency, preventing the recombination of electron-hole pairs, benefiting both pollutant oxidation and power generation. With the synergistic effect of photo-electrocatalysis and PMS-advanced oxidation, the PFC/PMS system can efficiently remove organic pollutants and/or inorganic nitrogen (especially NH_4^+-N) in freshwater via the function of ROS ($O_2•^-$, •OH and $^1O_2$) and $SO_4•^-$ as shown in Sheme 1 (left).

However, when applying the PFC/PMS system in marine environment, the common component of Cl^- could scavenge $SO_4•^-$ and •OH, making the mechanism much complicated. Typically, the ROSs and $SO_4•^-$ generated from intrinsic (photo-)catalytic PMS oxidation were rapidly consumed by excessive Cl^- via the reactions in Eqs. (14)-(25). The generation of $^1O_2$ from $O_2•^-$ was also inhibited by RCSs [53]. The transformation of these strong oxidative free radicals into less reactive species (such as $Cl_2•^-$ and Cl•) explained for the inherent bottleneck of applying traditional AOPs in (marine) saline wastewater treatment [62]. However, in this integrated PFC/PMS, synergies of (photo-)electrocatalytic chlorination and PMS-chlorination were spontaneously built up with the help of modified electrodes. The highly efficient generation of $HClO/ClO^-$ can partially compensate for the loss of oxidation capacity, promising satisfactory pollutant removal efficiency. Since the directly generation of $^1O_2$ from PMS was hardly affected by Cl^-, this non-radical pathway still played a leading role in organic pollutant removal. The generated oxidative chlorine species (HClO and ClO•) mainly functioned in inorganic nitrogen oxidation as the overall reaction of Eqs. (26)-(27). The detailed process of chlorine-mediated NH_4^+-N removal has been reported in our previous study [14].

$$\text{Cu-Co-WO}_3 + h\nu \rightarrow h^+ + e^- \quad (2)$$

$$H_2O + h^+ \rightarrow \bullet OH + H^+ \quad (3)$$

$$\equiv Cu^{2+}/Co^{3+}–OH^- + HSO_5^- \rightarrow \equiv Cu^{+}/Co^{2+}–\bullet OOSO_3^- + H_2O \quad (4)$$

$$2\equiv Cu^{+}/Co^{2+}–\bullet OOSO_3^- + 2\,H_2O \rightarrow 2\equiv Cu^{2+}/Co^{3+}–OH^- + {}^1O_2 + 2SO_4^{2-} + 2\,H^+ \quad (5)$$

$$\equiv Cu^{+}/Co^{2+} + HSO_5^- \rightarrow \equiv Cu^{2+}/Co^{3+} + SO_4•^- + OH^- \quad (6)$$

$$\equiv Cu^{2+}/Co^{3+} + HSO_5^- \rightarrow \equiv Cu^{+}/Co^{2+} + SO_5•^- + H^+ \quad (7)$$

$$\equiv Cu^{+} + HSO_5^- \rightarrow \equiv Cu^{3+} + SO_4^{2-} + OH^- \quad (8)$$

$$\equiv Cu^{3+} + OH^- \rightarrow \equiv Cu^{2+} + \bullet OH \quad (9)$$

$$\equiv Cu^{+} + \equiv Co^{3+} \rightarrow \equiv Co^{2+} + \equiv Cu^{2+} \quad (10)$$

$$HSO_5^- + SO_5^{2-} \rightarrow HSO_4^- + SO_4^{2-} + {}^1O_2 \quad (11)$$

$$SO_4•^- + H_2O \rightarrow SO_4^{2-} + \bullet OH + H^+ \quad (12)$$

$$SO_5•^- + SO_5•^- \rightarrow {}^1O_2 + 2SO_4^{2-} \quad (13)$$

$$Cl^- + h^+ \rightarrow Cl• \quad (14)$$

$$2Cl^- \rightarrow Cl_2 + 2e^- \quad (15)$$

$$HSO_5^- + 2Cl^- \rightarrow SO_4^{2-} + HOCl + Cl• \quad (16)$$

$$HOCl + Cl^- + H^+ \leftrightarrow Cl_2 + H_2O \quad (17)$$

$$SO_4•^- + Cl^- \rightarrow SO_4^{2-} + Cl• \quad (18)$$

$$\bullet OH + Cl^- \rightarrow HOCl^- \quad (19)$$

$$Cl• + Cl^- \rightarrow Cl_2•^- \quad (20)$$

$$Cl_2•^- + H_2O \rightarrow HOCl + Cl^- + H^+ + e^- \quad (21)$$

$$Cl_2•^- + Cl• \rightarrow Cl_2 + Cl^- \quad (22)$$

$$Cl_2 + H_2O \rightarrow HOCl + H^+ + Cl^- \quad (23)$$

$$HOCl/ClO^- + \bullet OH \rightarrow H_2O/OH^- + ClO• \quad (24)$$

$$HOCl/ClO^- + Cl• \rightarrow HCl/Cl^- + ClO• \quad (25)$$

$$2NH_4^+ + 3HOCl \rightarrow N_2 + 3\,H_2O + 5\,H^+ + 3Cl^- \quad (26)$$

$$NH_4^+ + 4HOCl \rightarrow NO_3^- + H_2O + 6\,H^+ + 4Cl^- \quad (27)$$

3.6. Technical superiorities and discussions in application

In this marine PFC/PMS system, photo-electrocatalysis, PMS-advanced oxidation and chlorination were integrated by the "bridge" of modified electrodes, which greatly expanded the application field of PFC. In the aspect of pollutant removal, higher removal rates of (refractory) organic pollutant and inorganic (ammonium) nitrogen in marine environment were achieved in this PFC/PMS system than in single PFC or PMS system, confirming the enhanced oxidation capacity via integrated (photo-)electrocatalytic chlorination and PMS-chlorination mechanism. In the aspect of energy consumption, the only electricity

input was 3.75 kWh m^{-3} for pumping, except for 2.5 W cm^{-2} of visible light illumination (can be substituted by sunlight). Besides, the system with high open circuit voltage (OCV) of 0.57 V can provide extra electricity during marine pollutant removal (146.0 mW m^{-3} in BC removal and 24.5 mW m^{-3} in BC + NH_4^+-N removal, under the resistance of 500 Ω), making this system competitive in energy-savings, comparing with the common electrochemical chlorination systems for advanced seawater treatment (Table 4). The relatively weak electric field also inhibited by-product generation by preventing the generation of excessive active chlorine. The remained free chlorine and chloramines in the treated water was much lower than the discharged standard for mariculture (Chinese industry standard, SC/T 9103–2007). The generated RCS from the interactions of free radicals during pollutant removal also endowed the system with disinfection potential [63]. Therefore, this PFC/PMS system is especially suitable for advanced treatment of mariculture wastewater.

To explore the practical application potential of this PFC/PMS system, mariculture solid wastes (MSW), derived from the feed residue, fish excreta and organism remains, were used as the natural carbon and nitrogen sources to prepare simulated mariculture wastewater. The fermentation contains 9.47 ± 0.13 mg L^{-1} of COD_{Mn} and 8.42 ± 0.23 mg L^{-1} of NH_4^+-N, together with 5.82 ± 0.83 mg L^{-1} of NO_3^--N and 0.17 ± 0.003 mg L^{-1} of NO_2^--N.

As expected, organic pollutants (COD_{Mn}) and inorganic nitrogen of

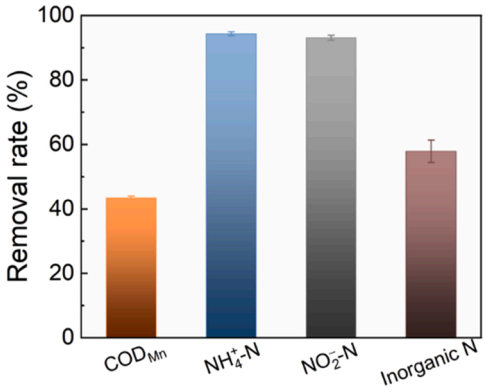

Fig. 9. Performance of the optimized PFC/PMS system in treating simulated mariculture wastewater with natural carbon and nitrogen sources.

Table 4
Comparison of electrochemical chlorine systems for mariculture wastewater treatment.

System	Electrodes	Wastewater	Target pollutants	Removal rates	Electricity supply	Energy consumption	Power generation	Ref.
PFC/PMS system (visible light)	Blue TNA anode & Cu-Co-WO_3 cathode	Simulated mariculture wastewater (with additional pollutants)	Berberine chloride (BC) = 10 mg L^{-1} NH_4^+-N = 10 mg L^{-1}	BC > 94% NH_4^+-N > 95%	None	None	146.0 mW m^{-3} for BC removal and 24.5 mW m^{-3} for BC + NH_4^+-N removal	This work
		Simulated mariculture wastewater (with natural carbon and nitrogen sources)	COD_{Mn} = 9.47 mg L^{-1} NH_4^+-N = 8.42 mg L^{-1} NO_2^--N = 0.17 mg L^{-1}	COD_{Mn} 43.43% NH_4^+-N 94.35% NO_2^--N 93.07%	None	None	38.72 mW m^{-3}	This work
Electrochemical system	Ti/IrO_2-SnO_2-Sb_2O_5 anodes & titanium plate cathodes	Actual mariculture wastewater	COD = 36.5 mg L^{-1} NH_4^+-N = 2.83 mg L^{-1} NO_2^--N = 2.98 mg L^{-1} SS = 46.2 mg L^{-1}	COD 79% NH_4^+-N 91% NO_2^--N 92% SS 91%	25 A m^{-2}	1.75kWh m^{-3}	None	[18]
Electrochemical oxidation system	Ti/RuO_2-IrO_2 anode & titanium plate cathode	Actual mariculture wastewater	COD_{Mn} = 24 mg L^{-1} NH_4^+-N = 5.23 mg L^{-1} NO_2^--N = 0.1 mg L^{-1} P = 0.5 mg L^{-1}	COD_{Mn} 48% NH_4^+-N 98% NO_2^--N 96% P 72%	5 mA cm^{-2}	0.27 kWh m^{-3} (0.056 kWh/g NH_4^+-N or 0.026 kWh/g COD)	None	[15]
Two-stage continuous chlorine electro-generation and breakpoint chlorination process	Ti/RuO_2 anode & Ti cathode	Simulated mariculture wastewater	NH_4^+-N = 10 mg L^{-1}	NH_4^+-N > 99%	33.4 A m^{-2}	1.21 × 10^{-5} kWh/mg NH_4^+-N	None	[64]
Electrochemical oxidation system	Boron doped diamond (BDD) anode and cathode	Recirculating mariculture wastewater	COD = 54.8 mg L^{-1} NH_4^+-N = 8 mg L^{-1} NO_2^--N = 80 mg L^{-1}	COD>35% NH_4^+-N > 99% NO_2^--N > 90%	10–50 A m^{-2}	0.33–0.78 kWh m^{-3}	None	[65]
Electrochemical oxidation system	Ti/IrO_2 anode & Ti cathode	Simulated mariculture wastewater	Norfloxacin = 125.0 μmol L^{-1}	Complete removal	6.53 mA cm^{-2}	Not given	None	[66]
Photo-electrochemical system (UV light)	Ti/SnO_2-Sb anode & carbon black air diffusion cathode	Simulated mariculture wastewater	Norfloxacin = 20 mg L^{-1}	TOC = 83.9%	5.2 mA cm^{-2}	Not given	None	[21]
Photo-electrocatalytic process (visible light)	MoS_2-3 @$BiVO_4$/FTO photoanode & Pt counter electrode & Ag/AgCl reference electrode	Artificial solution containing 0.1 mM NaCl	Bisphenol A = 10 ppm	Complete removal	1.5 V	Not given	1.75 mA cm^{-2}	[67]

NH_4^+-N and NO_2^--N were simultaneously oxidized to qualified level by the optimized PFC/PMS system in 30 min, with the delighted removal rates of 43.43%, 94.35% and 93.07%, respectively (Fig. 9). The system power generation was 38.72 mW m^{-3} with the cell voltage of 88 mV. Although the removal of NO_3^--N (which should be reductively removed) was not efficient enough (5%), its concentration was not further increased during NH_4^+-N and NO_2^--N oxidation, indicating the high nitrogen selectivity of the system. Therefore, this PFC/PMS system is suitable in treating mariculture wastewater commonly containing low-content organic pollutants (including refractory antibiotics) and oxidizable inorganic nitrogen (NH_4^+-N and NO_2^--N) [15]. In the circumstances when the reducible pollutants (such as nitrate nitrogen) become the main controlling factor, other technologies or system combination should be considered.

4. Conclusions

In this study, blue TNA anode and the Cu-Co-WO_3 cathode were simply prepared and modified in optical, electrochemical and catalytic performances, to construct an integrated PFC system for marine pollutant control. After optimizing the electrodes, PMS concentration, visible-light illumination and external resistance, this PFC/PMS system can simultaneously remove 94.18% of BC (10 mg L^{-1}, in 30 min) and 95.73% of NH_4^+-N (10 mg L^{-1}, in 30 min) in natural seawater to qualified level. The power generation, with the OCV of 0.57 V, made the system much energy-saving comparing with traditional electrochemical (chlorination) technologies. The roles of electrodes, PMS and Cl^- were investigated and a novel integrated mechanism was proposed, which can explain the inherent barrier/bottleneck when applying conventional AOPs (photo- or electro-catalysis and PMS-advanced oxidation) to seawater treatment, because of the present salt ions, especially the chloride. The synergy of (photo-)electrocatalytic chlorination and PMS-chlorination in natural seawater made this PFC/PMS system an alternative in treating high-salinity (marine) wastewater containing oxidative pollutants, including (refractory) organic pollutants and (ammonium and nitrous) nitrogen.

CRediT authorship contribution statement

Jiaqi Sun: Conduct test and analysis, Data curation, Formal analysis, Writing – original draft. **Lifen Liu:** System & concept design, Funding acquisition, Resources, Supervision, Writing – review & editing. **Fenglin Yang:** Supervision.

Declaration of Competing Interest

The authors declare that they have no known competing financial interests or personal relationships that could have appeared to influence the work reported in this paper.

Acknowledgements

This work was supported by the National Natural Science Foundation of China (No. 21677025).

Appendix A. Supporting information

Supplementary data associated with this article can be found in the online version at doi:10.1016/j.apcatb.2022.121215.

References

[1] J. Lu, J. Wu, C. Zhang, Y. Zhang, Y. Lin, Y. Luo, Occurrence, distribution, and ecological-health risks of selected antibiotics in coastal waters along the coastline of China, Sci. Total Environ. 644 (2018) 1469–1476.
[2] R. Zhang, Y. Kang, R. Zhang, M. Han, W. Zeng, Y. Wang, K. Yu, Y. Yang, Occurrence, source, and the fate of antibiotics in mariculture ponds near the Maowei Sea, South China: Storm caused the increase of antibiotics usage, Sci. Total Environ. 752 (2021), 141882.
[3] D. Zhang, A. Li, J. Xie, C. Ji, In vitro antibacterial effect of berberine hydrochloride and enrofloxacin to fish pathogenic bacteria, Aquac. Res. 41 (2010) 1095–1100.
[4] L. Wang, Y. Sun, B. Xu, G. Sagada, K. Chen, J. Xiao, J. Zhang, Q. Shao, Effects of berberine supplementation in high starch diet on growth performance, antioxidative status, immune parameters and ammonia stress response of fingerling black sea bream (Acanthopagrus schlegelii), Aquaculture 527 (2020), 735473.
[5] H.V. Doan, S.H. Hoseinifar, S. Jaturasitha, M.A.O. Dawood, R. Harikrishnan, The effects of berberine powder supplementation on growth performance, skin mucus immune response, serum immunity, and disease resistance of Nile tilapia (Oreochromis niloticus) fingerlings, Aquaculture 520 (2020), 734927.
[6] Q.F. Han, S. Zhao, X.R. Zhang, X.L. Wang, C. Song, S.G. Wang, Distribution, combined pollution and risk assessment of antibiotics in typical marine aquaculture farms surrounding the Yellow Sea, North China, Environ. Int. 138 (2020), 105551.
[7] J. Sun, N. Li, P. Yang, Y. Zhang, Y. Yuan, X. Lu, H. Zhang, Simultaneous antibiotic degradation, nitrogen removal and power generation in a microalgae-bacteria powered biofuel cell designed for aquaculture wastewater treatment and energy recovery, Int. J. Hydrog. Energy 45 (2020) 10871–10881.
[8] Y.Y. Peng, F. Gao, H.L. Yang, H.W. Wu, C. Li, M.M. Lu, Z.Y. Yang, Simultaneous removal of nutrient and sulfonamides from marine aquaculture wastewater by concentrated and attached cultivation of Chlorella vulgaris in an algal biofilm membrane photobioreactor (BF-MPBR), Sci. Total Environ. 725 (2020), 138524.
[9] D. Zheng, Q. Chang, Z. Li, M. Gao, Z. She, X. Wang, L. Guo, Y. Zhao, C. Jin, F. Gao, Performance and microbial community of a sequencing batch biofilm reactor treating synthetic mariculture wastewater under long-term exposure to norfloxacin, Bioresour. Technol. 222 (2016) 139–147.
[10] W. Song, Z. Li, Y. Ding, F. Liu, H. You, P. Qi, F. Wang, Y. Li, C. Jin, Performance of a novel hybrid membrane bioreactor for treating saline wastewater from mariculture: Assessment of pollutants removal and membrane filtration performance, Chem. Eng. J. 331 (2018) 695–703.
[11] J.H. Wang, J. Lu, J. Wu, Y. Zhang, C. Zhang, Proliferation of antibiotic resistance genes in coastal recirculating mariculture system, Environ. Pollut. 248 (2019) 462–470.
[12] S. Li, S. Zhang, C. Ye, W. Lin, M. Zhang, L. Chen, J. Li, X. Yu, Biofilm processes in treating mariculture wastewater may be a reservoir of antibiotic resistance genes, Mar. Pollut. Bull. 118 (2017) 289–296.
[13] J. Lu, Y. Zhang, J. Wu, J. Wang, C. Zhang, Y. Lin, Occurrence and spatial distribution of antibiotic resistance genes in the Bohai Sea and Yellow Sea areas, China, Environ. Pollut. 252 (2019) 450–460.
[14] J. Sun, L. Liu, F. Yang, Electro-enhanced chlorine-mediated ammonium nitrogen removal triggered by an optimized catalytic anode for sustainable saline wastewater treatment, Sci. Total Environ. 776 (2021), 146035.
[15] Z. Lang, M. Zhou, Q. Zhang, X. Yin, Y. Li, Comprehensive treatment of marine aquaculture wastewater by a cost-effective flow-through electro-oxidation process, Sci. Total Environ. 722 (2020), 137812.
[16] Y. Yang, J. Shin, J.T. Jasper, M.R. Hoffmann, Multilayer heterojunction anodes for saline wastewater treatment: design strategies and reactive species generation mechanisms, Environ. Sci. Technol. 50 (2016) 8780–8787.
[17] Z.-M. Song, L.-L. Yang, Y. Lu, C. Wang, J.-K. Liang, Y. Du, X.-Z. Li, Q. Hu, Y.-T. Guan, Q.-Y. Wu, Characterization of the transformation of natural organic matter and disinfection byproducts after chlorination, ultraviolet irradiation and ultraviolet irradiation/chlorination treatment, Chem. Eng. J. 426 (2021), 131916.
[18] Y. Xing, J. Lin, Application of electrochemical treatment for the effluent from marine recirculating aquaculture systems, Procedia Environ. Sci. 10 (2011) 2329–2335.
[19] C. Zhang, D. He, J. Ma, T.D. Waite, Active chlorine mediated ammonia oxidation revisited: Reaction mechanism, kinetic modelling and implications, Water Res. 145 (2018) 220–230.
[20] Q. Zhang, M. Zhou, X. Du, P. Su, W. Fu, G. Song, Highly efficient dual-cathode Electro-Fenton process without aeration at a wide pH range: simultaneously enhancing Fe(II) regeneration and mineralization efficiency, Chem. Eng. J. 429 (2022), 132436.
[21] H. Yu, D. Dou, X. Zhang, L. Zhang, H. Dong, H. Yu, Degradation of Norfloxacin in saline water by synergistic effect of anode and cathode in a novel photo-electrochemical system, J. Clean. Prod. 242 (2020), 118548.
[22] S. Xiao, J. Qu, X. Zhao, H. Liu, D. Wan, Electrochemical process combined with UV light irradiation for synergistic degradation of ammonia in chloride-containing solutions, Water Res. 43 (2009) 1432–1440.
[23] J. Yao, Y. Zhang, Z. Dong, Enhanced degradation of contaminants of emerging concern by electrochemically activated peroxymonosulfate: Performance, mechanism, and influencing factors, Chem. Eng. J. 415 (2021), 128938.
[24] Q. Wu, J. Cao, X. Wang, Y. Liu, Y. Zhao, H. Wang, Y. Liu, H. Huang, F. Liao, M. Shao, Z. Kang, A metal-free photocatalyst for highly efficient hydrogen peroxide photoproduction in real seawater, Nat. Commun. 12 (2021) 483.
[25] Y. Li, J. Sun, L. Liu, F. Yang, A composite cathode membrane with $CoFe_2O_4$–rGO/PVDF on carbon fiber cloth: synthesis and performance in a photocatalysis-assisted MFC-MBR system, Environ. Sci. Nano 4 (2017) 335–345.
[26] J. Cai, M. Zhou, Y. Pan, X. Du, X. Lu, Extremely efficient electrochemical degradation of organic pollutants with co-generation of hydroxyl and sulfate radicals on Blue-TiO_2 nanotubes anode, Appl. Catal. B 257 (2019), 117902.
[27] Y.-W. Choi, S. Kim, M. Seong, H. Yoo, J. Choi, NH_4-doped anodic WO_3 prepared through anodization and subsequent NH_4OH treatment for water splitting, Appl. Surf. Sci. 324 (2015) 414–418.

[28] S. Hilliard, G. Baldinozzi, D. Friedrich, S. Kressman, H. Strub, V. Artero, C. Laberty-Robert, Mesoporous thin film WO_3 photoanode for photoelectrochemical water splitting: a sol–gel dip coating approach, Sustain. Energy Fuels 1 (2017) 145–153.
[29] S.J. Hong, S. Lee, J.S. Jang, J.S. Lee, Heterojunction $BiVO_4/WO_3$ electrodes for enhanced photoactivity of water oxidation, Energy Environ. Sci. 4 (2011) 1781.
[30] N.E.P.A. Chinese, Water and Wastewater Monitoring Analysis Method, Fourth ed.,, Chinese Environmental Science Publishing Press, Beijing, 2002.
[31] V. Dutta, S. Sharma, P. Raizada, V.K. Thakur, A.A.P. Khan, V. Saini, A.M. Asiri, P. Singh, An overview on WO_3 based photocatalyst for environmental remediation, J. Environ. Chem. Eng. 9 (2021), 105018.
[32] V.T. Quyen, J. Kim, P.-M. Park, P.T. Huong, N.M. Viet, P.Q. Thang, Enhanced the visible light photocatalytic decomposition of antibiotic pollutant in wastewater by using Cu doped WO_3, J. Environ. Chem. Eng. 9 (2021), 104737.
[33] L. Cheng, T. Jiang, J. Zhang, Photoelectrocatalytic degradation of deoxynivalenol on CuO-Cu_2O/WO_3 ternary film: mechanism and reaction pathways, Sci. Total Environ. 776 (2021), 145840.
[34] N. Alizadeh, A. Salimi, T.-K. Sham, P. Bazylewski, G. Fanchini, F. Fathi, F. Soleimani, Hierarchical $Co(OH)_2$/FeOOH/WO_3 ternary nanoflowers as a dual-function enzyme with pH-switchable peroxidase and catalase mimic activities for cancer cell detection and enhanced photodynamic therapy, Chem. Eng. J. 417 (2021), 129134.
[35] A. Jena, T.R. Penki, N. Munichandraiah, S.A. Shivashankar, Flower-like porous cobalt(II) monoxide nanostructures as anode material for Li-ion batteries, J. Electroanal. Chem. 761 (2016) 21–27.
[36] X. Dai, Y. Dai, J. Lu, L. Pu, W. Wang, J. Jin, F. Ma, N. Tie, Cobalt oxide nanocomposites modified by NiCo-layered double hydroxide nanosheets as advanced electrodes for supercapacitors, Ionics 26 (2019) 2501–2511.
[37] C. Wang, F. Jiang, R. Zhou, Y. Du, P. Yang, C. Wang, J. Xu, Enhancement of methanol electrocatalytic oxidation on platinized WO_3–TiO_2 composite electrode under visible light irradiation, Mater. Res. Bull. 48 (2013) 1099–1104.
[38] L. Xu, J. Niu, H. Xie, X. Ma, Y. Zhu, J. Crittenden, Effective degradation of aqueous carbamazepine on a novel blue-colored TiO_2 nanotube arrays membrane filter anode, J. Hazard Mater. 402 (2021), 123530.
[39] Z. Ji, J. Wu, T. Jia, C. Peng, Y. Xiao, Z. Liu, Q. Liu, Y. Fan, J. Han, L. Hao, In-situ growth of TiO_2 phase junction nanorods with Ti^{3+} and oxygen vacancies to enhance photocatalytic activity, Mater. Res. Bull. 140 (2021), 111291.
[40] E.R. Sallam, H.M. Khairy, M.S. Elnouby, H.A. Fetouh, Sustainable electricity production from seawater using Spirulina platensis microbial fuel cell catalyzed by silver nanoparticles-activated carbon composite prepared by a new modified photolysis method, Biomass Bioenergy 148 (2021), 106038.
[41] Y. Yu, W. Xu, J. Fang, D. Chen, T. Pan, W. Feng, Y. Liang, Z. Fang, Soft-template assisted construction of superstructure TiO_2/SiO_2/g-C_3N_4 hybrid as efficient visible-light photocatalysts to degrade berberine in seawater via an adsorption-photocatalysis synergy and mechanism insight, Appl. Catal. B 268 (2020), 118751.
[42] M.C. DeRosa, R.J. Crutchley, Photosensitized singlet oxygen and its applications, Coord. Chem. Rev. 233–234 (2002) 351–371.
[43] X. Xiao, X. Shen, Contrastive analysis on content of chloride ion in different water, J. of Hunan University of Humanities, Sci. Technol., 140, 2014, pp. 133–137.
[44] C. Bai, G. Yang, S. Zhang, S. Deng, Y. Zhang, C. Chen, J. He, M. Xu, L. Long, A synergistic system of electrocatalytic-anode/α-MnO_2/peroxymonosulfate for removing combined pollution of tetracycline and Cr(VI), Chem. Eng. J. 423 (2021), 130284.
[45] J. Ding, H. Nie, S. Wang, Y. Chen, Y. Wan, J. Wang, H. Xiao, S. Yue, J. Ma, P. Xie, Transformation of acetaminophen in solution containing both peroxymonosulfate and chlorine: performance, mechanism, and disinfection by-product formation, Water Res. 189 (2021), 116605.
[46] Z. Wu, K. Guo, J. Fang, X. Yang, H. Xiao, S. Hou, X. Kong, C. Shang, X. Yang, F. Meng, L. Chen, Factors affecting the roles of reactive species in the degradation of micropollutants by the UV/chlorine process, Water Res. 126 (2017) 351–360.
[47] M. Antonopoulou, N. Ioannidis, T. Kaloudis, T.M. Triantis, A. Hiskia, Kinetic and mechanistic investigation of water taste and odor compound 2-isopropyl-3-methoxy pyrazine degradation using UV-A/Chlorine process, Sci. Total Environ. 732 (2020), 138404.
[48] M.J. Watts, K.G. Linden, Chlorine photolysis and subsequent OH radical production during UV treatment of chlorinated water, Water Res. 41 (2007) 2871–2878.
[49] C. Wei, B. Song, J. Yuan, Z. Feng, G. Jia, C. Li, Luminescence and Raman spectroscopic studies on the damage of tryptophan, histidine and carnosine by singlet oxygen, J. Photochem. Photobiol. A 189 (2007) 39–45.
[50] Y. Peng, H. Tang, B. Yao, X. Gao, X. Yang, Y. Zhou, Activation of peroxymonosulfate (PMS) by spinel ferrite and their composites in degradation of organic pollutants: a review, Chem. Eng. J. 414 (2021), 128800.
[51] D. Guo, Y. Wang, C. Chen, J. He, M. Zhu, J. Chen, C. Zhang, A multi-structural carbon nitride co-modified by Co, S to dramatically enhance mineralization of Bisphenol f in the photocatalysis-PMS oxidation coupling system, Chem. Eng. J. 422 (2021), 130035.
[52] C.-X. Li, C.-B. Chen, Y.-J. Wang, X.-Z. Fu, S. Cui, J.-Y. Lu, J. Li, H.-Q. Liu, W.-W. Li, T.-C. Lau, Insights on the pH-dependent roles of peroxymonosulfate and chlorine ions in phenol oxidative transformation, Chem. Eng. J. 362 (2019) 570–575.
[53] X. Wu, P. Liu, H. Wang, H. Huang, Y. Shi, C. Yang, S. Gao, Photo aging of polypropylene microplastics in estuary water and coastal seawater: Important role of chlorine ion, Water Res. 202 (2021), 117396.
[54] Y.F. Huang, Y.H. Huang, Behavioral evidence of the dominant radicals and intermediates involved in bisphenol A degradation using an efficient Co^{2+}/PMS oxidation process, J. Hazard Mater. 167 (2009) 418–426.
[55] H. Lee, H.-J. Lee, J. Jeong, J. Lee, N.-B. Park, C. Lee, Activation of persulfates by carbon nanotubes: oxidation of organic compounds by nonradical mechanism, Chem. Eng. J. 266 (2015) 28–33.
[56] J. Hou, S. Yang, H. Wan, H. Fu, X. Qu, Z. Xu, S. Zheng, Highly effective catalytic peroxymonosulfate activation on N-doped mesoporous carbon for o-phenylphenol degradation, Chemosphere 197 (2018) 485–493.
[57] X. Zhou, C. Luo, M. Luo, Q. Wang, J. Wang, Z. Liao, Z. Chen, Z. Chen, Understanding the synergetic effect from foreign metals in bimetallic oxides for PMS activation: a common strategy to increase the stoichiometric efficiency of oxidants, Chem. Eng. J. 381 (2020), 122587.
[58] Z. Li, Y. Sun, W. Huang, C. Xue, Y. Zhu, Q. Wang, D. Liu, Innovatively employing magnetic CuO nanosheet to activate peroxymonosulfate for the treatment of high-salinity organic wastewater, J. Environ. Sci. 88 (2020) 46–58.
[59] F. Jiang, B. Qiu, D. Sun, Advanced degradation of refractory pollutants in incineration leachate by UV/Peroxymonosulfate, Chem. Eng. J. 349 (2018) 338–346.
[60] J. Hao, S. Zhao, R. Mao, X. Zhao, Activation of peroxymonosulfate by cobalt doped graphitic carbon nitride for ammonia removal in chloride-containing wastewater, Sep. Purif. Technol. 271 (2021), 118858.
[61] Y. Hu, D. Chen, R. Zhang, Y. Ding, Z. Ren, M. Fu, X. Cao, G. Zeng, Singlet oxygen-dominated activation of peroxymonosulfate by passion fruit shell derived biochar for catalytic degradation of tetracycline through a non-radical oxidation pathway, J. Hazard Mater. 419 (2021), 126495.
[62] B. Sheng, Y. Huang, Z. Wang, F. Yang, L. Ai, J. Liu, On peroxymonosulfate-based treatment of saline wastewater: when phosphate and chloride co-exist, RSC Adv. 8 (2018) 13865–13870.
[63] T. Kohn, K.L. Nelson, Sunlight-mediated inactivation of MS_2 coliphage via exogenous singlet oxygen produced by sensitizers in natural waters, Environ. Sci. Technol. 41 (2007) 192–197.
[64] A. Romano, A.M. Urtiaga, I. Ortiz, Optimized energy consumption in electrochemical-based regeneration of RAS water, Sep. Purif. Technol. 240 (2020), 116638.
[65] V. Diaz, R. Ibanez, P. Gomez, A.M. Urtiaga, I. Ortiz, Kinetics of electro-oxidation of ammonia-N, nitrites and COD from a recirculating aquaculture saline water system using BDD anodes, Water Res. 45 (2011) 125–134.
[66] S.D. Jojoa-Sierra, J. Silva-Agredo, E. Herrera-Calderon, R.A. Torres-Palma, Elimination of the antibiotic norfloxacin in municipal wastewater, urine and seawater by electrochemical oxidation on IrO_2 anodes, Sci. Total Environ. 575 (2017) 1228–1238.
[67] Z. Zheng, Y.H. Ng, Y. Tang, Y. Li, W. Chen, J. Wang, X. Li, L. Li, Visible-light-driven photoelectrocatalytic activation of chloride by nanoporous MoS_2@$BiVO_4$ photoanode for enhanced degradation of bisphenol A, Chemosphere 263 (2021), 128279.